NANO LETTERS

2008
Vol. 8, No. 6
1778-1782

Magnetic Field Control of Exchange and Noise Immunity in Double Quantum Dots

M. Stopa*,† and C. M. Marcus‡

Center for Nanoscale Systems, and Department of Physics, Harvard University, Cambridge, Massachusetts 02138

Received May 5, 2008

ABSTRACT

We employ density functional calculated eigenstates as a basis for exact diagonalization studies of semiconductor double quantum dots, with two electrons, through the transition from the symmetric bias regime to the regime where both electrons occupy the same dot. We calculate the singlet−triplet splitting $J(\varepsilon)$ as a function of bias detuning ε and explain its functional shape with a simple, double anticrossing model. A voltage noise suppression "sweet spot," where $dJ(\varepsilon)/d\varepsilon = 0$ with nonzero $J(\varepsilon)$, is predicted and shown to be tunable with a magnetic field B.

The evolution of the phase of a quantum system in the presence of environmental noise, which has long been a subject of investigation in theoretical physics,[1] has acquired heightened significance with the emergence of quantum information processing and the prospect of quantum computing.[2] Control and manipulation of elementary quantum states, or qubits, can be devastated by fluctuations in system parameters which dephase the qubits.[3,4] Even when isolated qubits are immune from environmental noise, the initiation of interaction between qubits can introduce dephasing effects through the coupling Hamiltonian. The principle challenge now for the realization of robust quantum circuits is the design of single and multiple qubit evolution operators $U(\{X_i\})$, depending on a set of controllable parameters $\{X_i\}$, wherein we can locate generalized saddle points $\{\tilde{X}_i\}$ such that $\partial_{X_i} U(\{\tilde{X}_i\}) = 0$. In a seminal work, Vion et al.[5] devised a superconducting tunnel junction circuit based on the Cooper pair box, called the "quantronium", whose Rabi oscillation frequency was insensitive, to linear order, to variations in the magnetic flux and gate voltage control parameters.

Because of advanced fabrication technology and inherent scalability, semiconductor quantum dot systems present another promising candidate for quantum computation and information processing. The investigation of these systems has recently produced some auspicious results[6,7] by coherently manipulating and probing the spin and charge state of a small (typical electron number $N = 1$ and 2) system using (i) time-varying electric fields, (ii) charge sensors from nearby quantum point contacts,[8,9] and (iii) externally applied magnetic fields B. However, the problem of decoherence in quantum dot systems is also severe, and similar "optimum readout conditions" or "sweet spots" are necessary to achieve correctable quantum gate operations here as well.[4]

In this paper, we demonstrate the existence of a sweet spot in the singlet−triplet splitting $J(\varepsilon, B)$ in the regime studied in a recent experiment[6] where the two charge states of the double dot, $(N_L, N_R) = (1, 1),(0, 2)$ are near degeneracy. Here, B is the magnetic field[10] and ε is the "detuning" or bias difference between left and right dots whose occupancies are denoted N_L and N_R. We employ configuration interaction (CI) calculations of the structure studied in ref 6, with full geometric fidelity achieved by employing a CI basis derived from density functional theory (DFT) calculations for that device. We further develop a "double anti-crossing" model which analytically describes the sweet spot in terms of the basic coupling constants of the double dot and the control parameters.

Calculations using DFT for lateral heterostructures have been described extensively in the literature.[11] We correct the DFT single particle energies of the $N = 2$ double dot to avoid double counting of the Coulomb interaction which is diagonalized in the basis of Kohn−Sham states φ_i.[12] The advantage of this method is that the basis itself varies with gate voltages and B and thereby captures much of the evolving structure, much as a natural basis does in quantum chemistry.[13] The basis states are states of the full double dot, and so no artificial tunneling coefficient needs to be incorporated. Note that the Hartree−Fock model that we introduce below does, however, employ tunnel coefficients. Finally, the Coulomb matrix elements are calculated very efficiently with the kernel of Poisson's equation and therefore

* Corresponding author. E-mail: stopa@cns.fas.harvard.edu.
† Center for Nanoscale Systems, Harvard University.
‡ Department of Physics, Harvard University.

10.1021/nl801282t CCC: $40.75
Published on Web 05/22/2008

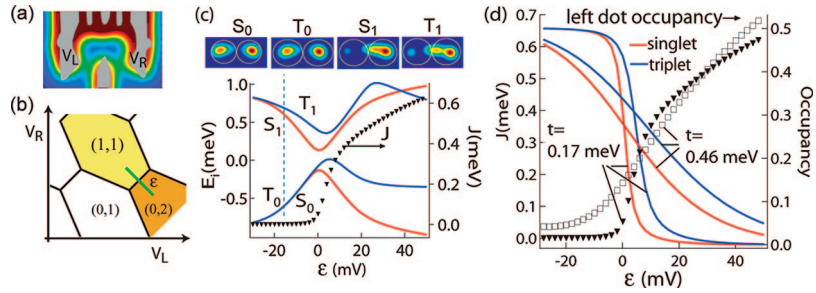

Figure 1. (a) Self-consistent effective 2D potential profile at 2DEG level, gate pattern superimposed; (b) schematic of honeycomb stability diagram indicating left and right gate voltage dependence (V_L, V_R, see also a). "Detuning" ε is denoted (positive to lower right). (c) Upper panel: lowest two singlet and triplet densities at large negative detuning (in the (1,1) region) with S_0 and T_0 showing (1,1) character and S_1 and T_1 having density mostly in right dot. Lower panel: CI energies and difference of lowest triplet and singlet J (triangles, right axis) versus detuning ε; (d) $J(\varepsilon)$ for two (singlet) tunnel coupling strengths t (triangles and boxes) and lowest singlet and triplet occupancies of left dot (right axis) for each t .

automatically include screening by the electrical environment.

The DFT self-consistent potential profile, with the device gate pattern superimposed,[14] is shown in Figure 1a. Here, the bias is approximately symmetric, and the potential minima of the two dots (~5 meV below the Fermi surface) are nearly equal. Experimentally, the two larger lateral gates, marked V_L and V_R, are typically used to impart the detuning; that is, $\varepsilon \propto V_L - V_R$. A schematic of the stability ("honeycomb") diagram in the plane of V_L and V_R is shown in Figure 1b. Figure 1c displays the CI-calculated lowest two singlet (S) and triplet (T) energies as a function of ε. The singlet and triplet ground states each anticross with their corresponding first excited states (the calculation preserves total spin). Also plotted is $J(\varepsilon) \equiv E_T^- - E_S^-$, where E_T^- and E_S^- are the triplet and singlet ground states, respectively. The nature of the four anticrossing states for $\varepsilon \approx -18$ mV (vertical blue dashed line) is shown by the total (2D) density plots in the upper panel of Figure 1c. Note that, even though we are on the (1,1) side of the anticrossings, $\varepsilon < 0$, the two excited states each have their densities concentrated in the right dot; that is, they are the states that become S and T (0,2) ground states for $\varepsilon > 0$. At the extreme left of Figure 1c, which is near the center of the (1,1) stability cell, the excited S and T states become degenerate. At this point, the excited states are not (0,2) states but are rather formed from orbitals above the first orbital in each dot.

Figure 1d exhibits $J(\varepsilon)$ for two interdot tunnel-coupling strengths. Also shown are the S (red) and T (blue) total occupancies of the left dot versus ε. The calculated results exhibit a coupling-dependent rapid increase of $J(\varepsilon)$, as experimentally observed. Additionally, in the (0,2) region ($\varepsilon > 0$), where the ε dependence of J was not published, the calculation predicts a saturation.

The structure of the numerical results in Figure 1c suggests that we can explain the shape of $J(\varepsilon)$ in terms of two overlapping anticrossings. These can be determined in their ideal form within a simple Hartree−Fock (HF) approximation where the four "bare" states are written[15] as $S_0 \equiv (L1\uparrow R1\downarrow)$, $S_1 \equiv (R1\uparrow R1\downarrow)$ (singlets) and $T_0 \equiv (L1\uparrow R1\uparrow)$, $T_1 \equiv (R1\uparrow R2\uparrow)$ (triplets). The single particle energies are written ε_{R1}, ε_{L1}, and ε_{R2} (ε_{L2} is not used). We include the electrostatic potentials of the dot potential minima, $eC\varphi_L$ and $eC\varphi_R$ in the bare level energies (here C is a gate-to-dot lever arm, assumed constant); hence $\varepsilon_{L1} = \varepsilon_{L1}^0 + eC\varphi_L$, where ε_{L1}^0 denotes the energy measured from the dot bottom. Similar expressions hold for the other level energies. Within an HF type description, the bare eigenfunctions are retained, and the energies are shifted by direct and exchange Coulomb matrix elements. Thus, we write $E_S^0 = \varepsilon_{L1} + \varepsilon_{R1} + V_{inter} + V_{inter}^{ex}$, $E_S^1 = 2\varepsilon_{R1} + V_{intra} + V_{intra}^{ex}$, $E_T^0 = \varepsilon_{L1} + \varepsilon_{R1} + V_{inter} - V_{inter}^{ex}$, and $E_T^1 = \varepsilon_{R1} + \varepsilon_{R2} + V_{intra} - V_{intra}^{ex}$. For simplicity, we ignore the state-dependence of the inter- and intra-dot matrix elements. In fact, V_{intra} is necessarily greater for both electrons in the R1 orbital than for one in R1 and one in R2. This dependence tends to lower the triplet energy relative to the singlet. The singlet−triplet crossing in a single dot,[18] which is crucial to the existence of a sweet spot and is discussed below, is thereby shifted to lower magnetic field. Since the single particle level spacing, on which the singlet−triplet splitting also depends, is only a parameter in this Hartree−Fock description, there is no qualitative error from ignoring the matrix element state dependence, and for quantitative results, we are relying on the full CI calculations in any case.

The anticrossing of the singlets results from the tunnel coupling of the two single particle ground states which we denote t_{11}. However, crucially, the triplets anticross with tunnel coupling t_{12}, since the R1 state is blocked by the Pauli principle. Because of the humped shape of the barrier, tunneling from L1 to the higher R2 is stronger ($t_{12} > t_{11}$), and this is evident in Figure 1c. The two branches of the singlet and triplet are found by diagonalizing the standard 2 × 2 determinants:

$$E_{S\pm} = \tilde{E}_S \pm 0.5\sqrt{(C\varepsilon)^2 + 4t_{11}^2}$$
$$E_{T\pm} = \tilde{E}_T \pm 0.5\sqrt{(C\varepsilon - \delta)^2 + 4t_{12}^2} \quad (1)$$

where $\tilde{E}_T \equiv (E_T^0 + E_T^1)/2$ and $\tilde{E}_S \equiv (E_S^0 + E_S^1)/2$. Here, ε is defined relative to the detuning at which $E_S^1 = E_S^0$; $\varepsilon_0 \equiv \varepsilon_{R1}^0 - \varepsilon_{L1}^0 - V_{inter} + V_{intra} - V_{inter}^{ex} + V_{intra}^{ex}$. Also, δ is the detuning at which $E_T^1 = E_T^0$, relative to ε_0. It is given by $\delta = \varepsilon_{R2}^0 - \varepsilon_{R1}^0 - 2V_{intra}^{ex} + 2V_{inter}^{ex}$. The singlet−triplet splitting is the difference between the two lower branches in eq 1:

$$J(\varepsilon) = \widetilde{E}_T - \widetilde{E}_S - 0.5\sqrt{(C\varepsilon - \delta)^2 + 4t_{12}^2} + 0.5\sqrt{(C\varepsilon)^2 + 4t_{11}^2} \quad (2)$$

note that $\tilde{E}_T - \tilde{E}_S$ is independent of ε.

Figure 2a shows the HF energies for the few levels, $E_{S\pm}$, $E_{T\pm}$. Away and to the left of the anticrossings, the gap between the ground states S and T is $E_T^0 - E_S^0 \equiv \Delta_{ST}(1, 1) = -2V_{inter}^{ex}$. The gap between the (bare) excited states is $E_T^1 - E_S^1 \equiv \Delta_{ST}(0, 2) = \varepsilon_{R2} - \varepsilon_{R1} - 2V_{intra}^{ex}$; that is, it depends on a single particle level spacing in dot R.[16] Clearly, from Figure 2b, as J increases near $\varepsilon = 0$, so too does $dJ/d\varepsilon$. For spin manipulation with noise immunity, it would be advantageous to find a regime where J was appreciable but $dJ/d\varepsilon$ was not. This turns out to be possible as we show below. In Figure 2b, we also fit $J(\varepsilon)$ from Figure 1d (i.e., the full CI results, specifically the curve with the smaller dot−dot coupling) with eq 2. The fit is good as long as points far into the (0,2) region are excluded. Here, the potential confinement begins to change and the bare level spacing is no longer constant. We have also fit the expression eq 2 to unpublished data, at $B = 0$, from the device in ref 6 (not shown) and found values of $t_{11} \approx 0.3$ meV, $C \approx 12$, and $\delta \approx 4.6$ mV.[17] Since the triplet anticrossing occurs so far from the singlet anticrossing, the fitted value of t_{12} is not significant.

Two additional notes regarding t_{11} versus t_{12} are the following. Single particle level R2 in a circular dot is doubly degenerate. Any dot ellipticity will lower one of these degenerate states relative to the other. The geometric orientation of the two states can strongly affect their

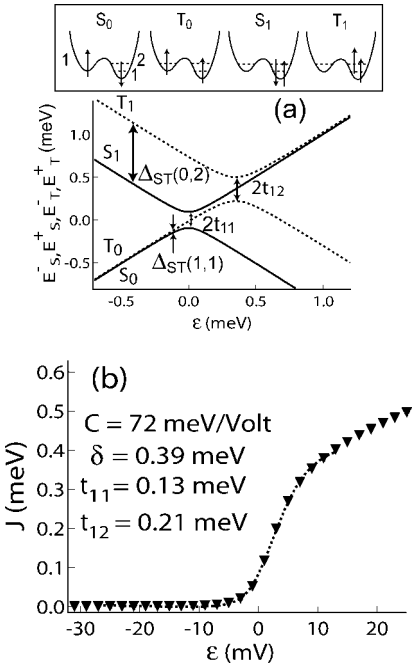

Figure 2. (a) Schematic of double anticrossing near (1,1) to (0,2) transition. Singlets (solid) anticross with t_{11}; triplets (dashed) anticross with t_{12}. Singlet−triplet splitting of ground ($\Delta_{ST}(1, 1)$) and excited ($\Delta_{ST}(0, 2)$) states in (1,1) region indicated. Top box: schematic of the configurations of the four anticrossing states. (b) Fit of calculated $J(\varepsilon)$ to anticrossing eq 2 (dashed line) for $t = 0.17$ meV case in Figure 1. Triangles reproduce points in Figure 1c.

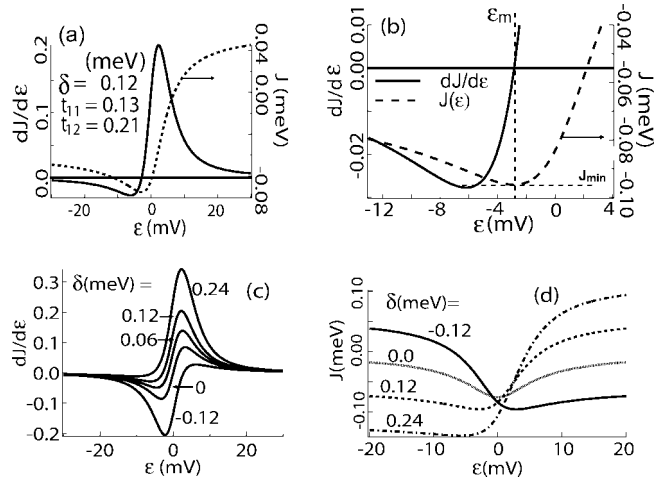

Figure 3. (a) $dJ/d\varepsilon$ (solid, left scale) and $J(\varepsilon)$, from eqs 3 and 2, respectively, for tunnel and δ parameters in Figure 2b. Note, offset energies, $\tilde{E}_S$, $\tilde{E}_T$, taken as zero throughout the figure, so offsets of J are arbitrary. Expanded view in b shows minimum ($dJ(\varepsilon_m)/d\varepsilon \equiv 0$) and depth of minimum. As $\varepsilon \to -\infty$, J saturates above the figure. For same tunnel coefficients, $dJ/d\varepsilon$ (c) and $J(\varepsilon)$ (d), for a range of values of δ. Minimum of $J(\varepsilon)$ (i.e., ε_m) switches sign to positive when δ changes sign to negative.

couplings to the neighboring, L1, state. Thus, while energetically we expect $t_{11} < t_{12}$, if the p axis (line of the wave function lobes) of the lower R2 state is perpendicular to the axis between the dots, the case of $t_{11} > t_{12}$ could be realized. Second, in a magnetic field B (discussed below), the two branches of R2 split, and the lower branch moves toward degeneracy with R1, causing $t_{12} \to t_{11}$ as $B \to \infty$. However, the singlet−triplet degeneracy in a single dot (again, see below) is facilitated by exchange and does not actually necessitate $\varepsilon_{R2}^0 = \varepsilon_{R1}^0$. Hence, the physics of the sweet spot occurs when the R1 and R2 levels are still significantly different. Note also that the full self-consistent calculations do not employ tunnel parameters and so automatically take these features into account.

In what follows, we show that eq 2 has exactly one extremum, $dJ/d\varepsilon = 0$, except where $t_{11} = t_{12}$. We then show in what parameter region the extremum is a minimum and how the parameters can be modulated by magnetic field B to control the minimum.

First, to show that $J(\varepsilon)$ has a single minimum, we take the derivative of eq 2:

$$\frac{dJ}{d\varepsilon} = -0.5\frac{(C\varepsilon - \delta)}{\sqrt{(C\varepsilon - \delta)^2 + 4t_{12}^2}} + 0.5\frac{C\varepsilon}{\sqrt{(C\varepsilon)^2 + 4t_{11}^2}} \quad (3)$$

and observe that the two terms are sigmoidal curves which (for $t_{11} \neq t_{12}$) must intersect in one point, specifically $\varepsilon_m = \delta/(1 - (t_{12}/t_{11}))$. A second derivative test shows that, for $t_{12} > t_{11}$ (the usual case), the extremum is a minimum. Note also that, assuming $t_{12} > t_{11}$, $\delta > 0 \Longrightarrow \varepsilon_m < 0$ (the minimum is in the (1,1) zone; compare with Figure 1b) and $\delta < 0 \Longrightarrow \varepsilon_m > 0$.

Evaluating the depth D of the minimum of $J(\varepsilon)$ yields $D \equiv J(\varepsilon_m) - J(\varepsilon \to -\infty) = 0.5\delta(1 - \sqrt{1+4|t_{12}-t_{11}|^2/|\delta|^2}) \approx |t_{12} - t_{11}|^2/|\delta|$. The full CI calculations, which include the realistic interdot barrier, allow us to estimate the tunnel

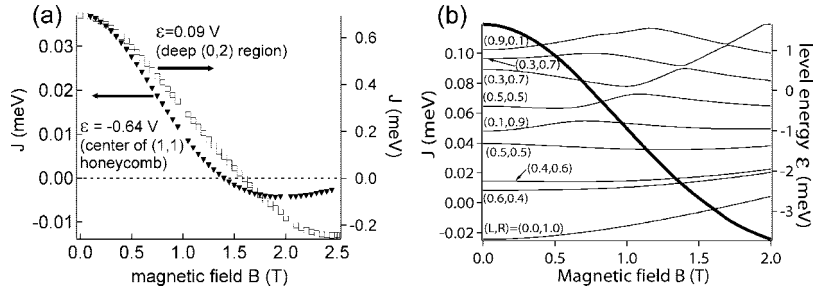

Figure 4. (a) Magnetic field dependence of J, from full CI calculations, for center of (1,1) honeycomb cell (i.e., balanced gate voltages), triangles, and for strong (0,2) regime where both electrons occupy right dot, boxes. Note carefully the difference between left and right scales. Single dot requires greater B to drive S−T transition, but $|dJ/dB|$ is much greater in (0,2). (b) Kohn−Sham level energies and J versus B at fixed detuning near (0,2) to (1,1) degeneracy. Fraction of wave function on (left,right) dot indicated for each level.

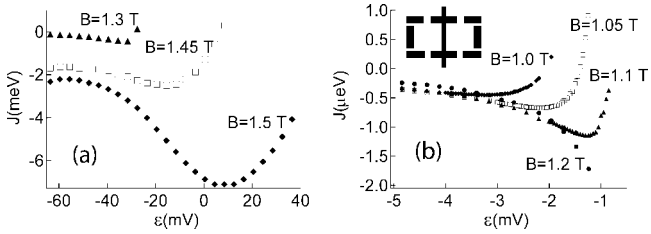

Figure 5. Full CI calculation for $J(\varepsilon)$ for various B for two gate patterns. (a) The device from ref 6 and (b) a "bar" style gate pattern depicted in the inset of b. The latter case is characterized by a smaller single particle level spacing and much weaker tunnel coupling. For these values of B, the sweet spot in b has a value in microelectronvolts.

coefficients (compare Figure 1c where the singlet and triplet anticrossings have gaps of $2t_{11}$ and $2t_{12}$, respectively). Here and in comparable parameter ranges, the tunnel coefficient ratio $t_{12}/t_{11}\sim 1.3$. Figure 3 shows $J(\varepsilon)$ and its derivative for various values of the parameters δ, t_{11}, and t_{12} as calculated from eq 2.

From its definition, δ is the level spacing of dot R corrected by the inter- and intradot exchange energies and, at $B = 0$, is of order 1.2 meV from calculations for the device in ref 6. Note that δ forms the major portion of $\Delta_{ST}(0, 2)$ (cf. Figure 2a) and that if we can reduce $\Delta_{ST}(0, 2)$ while keeping $\Delta_{ST}(1, 1)$ relatively fixed this will cause the two anticrossings to move closer to one another. This is achieved as follows.

For nonzero B, direct paramagnetic interaction on the orbital angular momentum splits the branches of the first excited single particle state, and Hund's coupling can induce a transition in the $N = 2$ single dot, (0,2), to a triplet ground state; see Figure 4 and ref 18. As shown in Figure 4, this magnetic field influence on J deep in the (0,2) region is greater than that in the (1,1) zone.[12,19] It is this difference of the coupling of B to the two splittings, $\Delta_{ST}(0, 2)$ and $\Delta_{ST}(1, 1)$, that allows for a sensitive tuning of the sweet spot with B as shown in Figure 5.

We display the full CI results, exhibiting the sweet spot evolution with B, in Figure 5 for the double dot shown in Figure 1a in the strong coupling case ($t \approx 0.46$ meV) and, for comparison, with another double dot pattern (inset Figure 5b) with gates set at much weaker coupling, $t \approx 0.03$ meV. The geometrical features which influence the location of the sweet spot include the tunnel coupling as well as the dot level spacings $\delta\varepsilon$ and the "breadth" of the wave function,[12] which affects the exchange interaction. Here, $\delta\varepsilon$ is smaller for the second ("bar") gate pattern. The motion of the minimum with B is much greater when tunneling is stronger, Figure 5a. In Figure 5a the sweet spot crosses into the (0,2) zone (cf. Figure 1b) close to where the triplet anticrossing and singlet anticrossing coincide. This and most other features of the full CI calculation can be modeled with the parameters of the double-anticrossing HF model. Further, gate voltages and gate patterns can be tuned to robustly move the sweet spot around and deepen it or make it more shallow. One feature, however, which is not explained by the HF model is the following. In both of the gate-patten cases investigated here, no minimum of J appears until B is large enough to produce a near degeneracy of the (0,2) singlet and triplet. Presumably, this results from the inadequacy of the double-anticrossing model when the two anticrossings are widely separated and other levels become important.

Finally, concerning the significance and efficacy of eliminating the linear component of fluctuating voltages, we note that the relevant time scale for quantum computation in dots is set by the period of Rabi oscillations. According to our calculations, $|J|$, at the sweet spot, can be made of order 1 meV suggesting a Rabi period $\tau_E = \pi\hbar/J \approx 2$ ps. The thermal noise associated with the circuitry can be estimated as equivalent to a temperature of 1 K and a resistance of 50 Ω, or about 5×10^{-8} mv/$\sqrt{\text{Hz}}$.[20] This suggests that errors induced by the curvature of $J(\varepsilon)$ at the sweet spot (typically, cf. Figure 5, the curvature is $\alpha \sim 10^{-3}$ meV/mv^2) are presumably negligible. However, in this limit, the electrical fluctuations are themselves negligible. A more serious problem might be related to charge switching noise[21,22] where a fluctuation of tens of microelectronvolts on a time scale of microseconds is possible. For this type of noise, we expect that operation at the sweet spot could result in significant enhancement of fidelity.

In summary, we have demonstrated that device parameters can be tuned near the (1,1) to (0,2) crossover to generate a relatively noise-immune sweet spot where the singlet−triplet splitting $J(\varepsilon)$ exhibits a minimum. The depth of the minimum, $\sim|t_{12} - t_{11}|^2/|\delta|$, and its detuning value, $\varepsilon_m = \delta/(1 - (t_{12}/t_{11}))$, can be modulated with magnetic field and tunnel barrier height. The existence of this noise-immune point for spin

interactions is a promising development for quantum dot quantum computation.

Acknowledgment. We acknowledge the National Nanotechnology Infrastructure Network Computation project, NNIN/C, for computational resources. C.M.M. acknowledges support from DARPA under QUIST and the ARO/DTO. We thank David Reilly, Edward Laird, Jason Petta, Jacob Taylor, Yasuhiro Tokura, and Amir Yacoby for helpful conversations.

References

(1) (a) Bray, A. J.; Moore, M. A. *Phys. Rev. Lett.* **1982**, *49*, 1545. (b) Caldeira, A. O.; Leggett, A. J. *Phys. Rev. A* **1985**, *31*, 1059.
(2) (a) Nielsen, M. A.; Chuang, I. L. *Quantum Computation and Quantum Information*, Cambridge University Press: Cambridge, 2000. (b) Vandersypen, L. M. K., Ph.D. Thesis, Stanford University, July, 2001.
(3) Coish, W. A.; Loss, D. *Phys. Rev. B* **2005**, *72*, 125337.
(4) Hu, X.; Das Sarma, S. *Phys. Rev. Lett.* **2006**, *96*, 100501.
(5) Vion, D.; et al. *Science* **2005**, *296*, 886.
(6) Petta, J.; et al. *Science* **2005**, *309*, 2180.
(7) (a) Hanson, R.; et al. *Phys. Rev. Lett.* **2005**, *94*, 196802. (b) Johnson, A. C.; et al. *Nature* **2005**, *435*, 925. (c) Koppens, F. H. L.; et al. *Science* **2005**, *309*, 1346. (d) Hatano, T.; Stopa, M.; Tarucha, S. *Science* **2005**, *309*, 268. (e) Hatano, T.; Stopa, M.; Yamaguchi, T.; Ota, T.; Yamada, K.; Tarucha, S. *Phys. Rev. Lett.* **2004**, *93*, 066806. (f) Elzerman, J. M.; et al. *Nature* **2004**, *430*, 431.
(8) Field, M.; et al. *Phys. Rev. Lett.* **1993**, *70*, 1311.
(9) Elzerman, J. M.; et al. *Phys. Rev. B* **2003**, *67*, 161308.
(10) The magnetic field is applied perpendicular to the device plane and only orbital (i.e. not Zeeman) effects are included.
(11) (a) Stopa, M. *Phys.Rev. B* **1996**, *54*, 13767. (b) Stopa, M. *Semicond. Sci. Technol.* **1998**, *13*, A55. (c) Burkard, G.; Loss, D.; DiVincenzo, D. *Phys. Rev. B* **1999**, *59*, 2070. (d) Szafran, B.; Peeters, S.; Bednarek, S. *Phys. Rev. B* **2004**, *70*, 205318. (e) Melnikov, D.; et al. *Phys. Rev. B* **2006**, *70*, 041309.
(12) van der Wiel, W.; et al. *New Journal of Physics* **2006**, *8*, 28.
(13) (a) Löwdin, P. *Phys. Rev.* **1955**, *97*, 1474. (b) Fulde, P. *Electron Correlations in Molecules and Solids*; Springer: Berlin, Heidelberg, 1995.
(14) Ciorga, M.; et al. *Phys. Rev. B* **2000**, *61*, R16315.
(15) We use "1" and "2" to denote the lowest two single particle levels localized in one or the other dot.
(16) To clarify the notation, $\Delta_{ST}(0, 2)$ is here defined as the splitting between the singlet and the triplet excited states in the (1,1) region of the stability diagram, i.e. for $\varepsilon < 0$. It is denoted "(0,2)" because these two excited states each have two electrons on the right dot (cf. S_1 and T_1 in top panel of Figure 1c).
(17) Edward Laird, private communication.
(18) Sasaki, S.; et al. *Nature (London)* **2000**, *405*, 764.
(19) (a) Hu, X.; Das Sarma, S. *Phy. Rev. A* **2000**, *61*, 062301. (b) Stopa, M. *Physica E* **2001**, *10*, 103.
(20) David Reilly, private communication.
(21) Fujisawa, T.; Hirayama, Y. *Appl. Phys. Lett.* **2000**, *77*, 543.
(22) Lu, W.; et al. *Nature* **2003**, *423*, 422.

NL801282T